Transient evolution of the target erosion profile during magnetron sputtering: dependence on gas pressure and magnetic configuration

Takeo Nakano[a,*], Yudai Saitou[a], Kei Oya[a]

[a] *Dept. of Materials and Life Science, Seikei University, 3-3-1, Kichijoji-Kita, Musashino, Tokyo, 180-8633, Japan*

Abstract

The growth of the target erosion profile (racetrack) in DC magnetron sputtering has been experimentally studied at a modest target power. Unbalanced magnetron sputtering (UBMS) and balanced magnetron sputtering (BMS) of a copper target were conducted at Ar gas pressures between 0.38 $\sim$ 2.0 Pa at a constant DC discharge power of 100 W. At time intervals of several hours throughout the target life, the target was removed from the chamber, and its erosion profile was measured with a height gauge. The racetrack width was found to have an interesting pressure dependence. Higher argon gas pressure resulted in a wider initial track width in both the UBMS and BMS configurations. As the sputter erosion of the target proceeded, the track width became narrower at higher gas pressures ($\geq$ 1.0 Pa). At lower gas pressures, the track width was mostly unchanged and even showed a slight increase in the case of 0.38 Pa in UBMS. As a result, the order of the final width was reversed: the higher gas pressure resulted in a narrower track width. The origin of this behavior was ascribed to the difference in the plasma sheath thickness and the free path of secondary electrons.

Keywords: magnetron sputtering, target erosion, gas pressure

PACS: 52.77.Dq, 52.80.Sm, 81.15.Cd

*Corresponding author

Email addresses: nakano@st.seikei.ac.jp (Takeo Nakano), yudai@surf.ml.seikei.ac.jp (Yudai Saitou), k.oya@st.seikei.ac.jp (Kei Oya)

1. Introduction

The planar magnetron sputter deposition system, invented by Chapin in the 1970s [1, 2], has become a preferred process in the vacuum coating industry [3, 4, 5, 6]. This deposition system utilizes an arched-shape magnetic field above the sputtering cathode to modify the motion of secondary electrons into the cycloid-like trajectory known as the $E \times B$ drift in plasma physics. Without the magnetic field, secondary electrons are accelerated along the target normal and reach the confronted substrate with a straight trajectory. Therefore, at lower gas pressures, where the mean free path (MFP) of the electrons is long, most electrons cannot contribute to the ionization of the sputtering gas, and the discharge is barely maintained. In addition, the heavy thermal load on the substrate as a result of high-energy electron bombardment has been a problem in conventional diode sputtering systems. The modified electron trajectory extends the electron path and suppresses substrate bombardment, which increases the ionization events and alleviates the thermal load, respectively [7, 8].

One serious drawback of planar magnetron sputtering is the inhomogeneous sputter-etching of the target, which results in the formation of a "racetrack"-like erosion profile. This inhomogeneous etching is a result of localized plasma distribution due to the arched magnetic field, which produces a non-uniform flux profile of positive ions that sputter the target material. As discussed in Chapin's initial study [1], the racetrack formation determines the target lifetime and the efficiency of the material usage. Therefore, this problem has attracted the interest of many researchers.

Plasma simulation studies have been actively performed using various techniques in order to predict the erosion profile based on the system configuration and experimental parameters. These studies include a Monte Carlo (MC) approach to track secondary electron motion and ionization events [9, 10, 11, 12, 13], an MC plus relaxation continuum model [14, 15] (and the model that additionally uses the Boltzmann equation for ions [16]), a simplified MC model

of high-energy electrons across trajectory domains [17], and full particle-in-cell MC collision (PIC-MCC) simulations [18, 19, 20, 21, 22]. Good reviews on this topic have been given by Kadlec [23] and Bogaerts *et al.* [24]. An analytical approach has recently been proposed that treats the secondary electron path in accordance with the magnetic flux lines [25]. In spite of these researches, the study of this field is incomplete and still in progress.

In general, simulations have reproduced the experimental results adequately, but not completely. The peak position could be predicted well, but the prediction of the erosion shape has been rather poor. We consider that a possible reason for the poor erosion shape prediction is the simplified boundary conditions used in plasma simulation studies. Most studies assumed the target surface to be a flat boundary and compared the simulation results (ion flux distributions onto the target) with experimentally obtained erosion profiles. In many cases, the erosion profile was only a single "snapshot" within the target lifetime (primarily at the end of the target lifetime), and the effect of the target surface geometry evolution on the generated magnetron plasma was ignored.

Experimental approaches to understanding the racetrack formation are rather scarce in comparison with simulation studies. Fukami *et al.* observed the target erosion pattern by means of the difference in the target surface appearance in reactive sputtering and found a wider erosion width in the cases of higher gas pressure (at a constant discharge voltage) and higher discharge voltage (at a constant pressure) [26]. The magnetic field configuration dependence of the erosion area was also studied by Fukami *et al.*, and it was found that the erosion gradually decreased towards the center and the erosion width became narrower as the field configuration changed from a balanced field to an unbalanced one [27]. Their results were interesting and comprehensive. However, the magnetic field strength used ($\sim$ 100 G) in their study was relatively weak in comparison with that used today, and the transient evolution of the profiles was not discussed.

There have been a series of experimental studies aimed at achieving more efficient target usage by modifying the magnetic configuration, which were well reviewed in the report by Musil *et al.*[28] Among these, the moving magnet

system has become the most commonly used and actively studied [29, 30, 31, 32]. However, it is difficult to compare the results of these experiments with simulations based on a static magnetic field.

We have, therefore, attempted to measure the evolution of the target erosion profile. In a previous report [33], the target erosion profile generated in an unbalanced magnetron sputtering (UBMS) apparatus has been measured for Al and Cu targets in Ar gas pressures of 0.38 $\sim$ 1.0 Pa. The track width was found to change as the erosion proceeded: the width increased at 0.38 Pa and decreased at 1.0 Pa for both elements. The erosion profile evolutions were similar between Al and Cu targets, except for the difference in erosion growth rates, reflecting the difference in sputtering yields between these materials [34].

In this study, we extended our experimental study to include the balanced magnetron sputtering (BMS) apparatus and carefully compared the erosion profiles. We selected only Cu targets for this study because of the similarity between the Al and Cu results in the previous study. Clear dependences on the gas pressure and magnetron configuration were confirmed, and the origin of these dependencies was discussed.

2. Experimental

The sputter chamber used in this study was a cylinder with 201-mm diameter and 201-mm height. It was equipped with a magnetron sputter cathode positioned at the symmetric axis of the chamber. Copper disks of 75-mm diameter and 5-mm thickness were used as sputtering targets. The targets were sliced from copper rods (JIS C 1020) and polished for use as sputtering targets. In some batches, a sintered target (Furuuchi Chemical, CUT-20363B) was used to confirm the effect of the target preparation. The distance between the target surface and the top plate of the chamber was 82 mm. In this study, no substrate holder was introduced in the chamber.

[Figure 1 about here.]

The magnet configuration was also axisymmetric. Before the sputtering experiment, we removed each magnet from the magnetron cathode and measured the magnetic field profiles with a gauss meter (F. W. Bell, model 4048) by moving the probe laterally at different heights in 5-mm steps. The results within the r–z plane are shown in Figure 1. The dot–dashed arrow at the left of the figure shows the symmetric axis. Along with the vector map of the magnetic field profile, the cathode, target, and shield (anode) of the sputter gun are also displayed in the figure.

In general, the maximum ionization in magnetron plasma occurs where the magnetic flux vector $\vec{B}$ is parallel to the target [7]. In other words, ions are frequently generated where the z-component of the magnetic field (B_z) is zero. Because ions are heavy and are not significantly affected by the magnetic field, they are accelerated straight down to the target and cause sputtering. Therefore, extensive erosion occurs under these locations. In UBMS, the magnetic flux is unbalanced between the south-pole center magnet and the north-pole ring magnet. Therefore, the $B_z = 0$ positions tend to lie nearer to the symmetric axis. In addition, as the $B_z = 0$ line leaves the target surface, its radial position bends inward to the center. On the other hand, in BMS, the magnetic flux lines are closed in both poles, and the $B_z = 0$ positions lie on a straight line perpendicular to the target surface at $r \approx 18$ mm, which is a larger radius than that of the UBMS configuration.

The chamber was routinely evacuated down to 5×10^{-5} Pa by a turbomolecular pump. After the evacuation, Ar gas was introduced into the chamber through a mass flow controller to achieve gas pressures of 0.38, 0.50, 1.0, and 2.0 Pa. The gas pressure was measured by a capacitance manometer (Megatorr, CDLD-0107J). Then, a DC power of 100 W was applied by a power source (MDX-500, Advanced Energy), and the magnetron discharge was generated. The target voltage was recorded during the sputtering.

At time intervals of several hours, the target was removed from the chamber, placed on a linear stage, and its erosion profile was measured with a height gauge (resolution 0.01 mm). The profiles were obtained along two orthogonal

diameters that were fixed throughout the sputtering of the target. The height data of the target surface was recorded with 0.5–2 mm lateral steps. We made a small depression at a peripheral part of the fresh target surface, and we carefully reproduced the position of the target on the sputter gun during repeated sputtering and profile measurements. The reproducibility of the position was estimated to be better than 0.3 mm in lateral directions, and 1° along the rotational coordinate.

After the measurement, the tilt of the target surface was removed using several data points at both ends of the surface, where the clamp ring of the target resides. The line constructed by these points was regarded as the baseline of the depth profile. This procedure was repeated until the depth of the erosion profile peak exceeded 4 mm (the original target thickness was 5 mm).

In UBMS discharges, plasma diagnostics were obtained using the Langmuir probe (Scientific Systems, SmartProbe) to evaluate the basic plasma parameters (electron density and temperature). The probe was a tungsten wire with 0.38-mm diameter and 10-mm exposure length from the insulator sleeve. The probe was introduced along the symmetric axis of the system, and its apex was located 10 mm from the target during the measurement.

3. Results and Discussion

[Figure 2 about here.]

Figure 2 shows several snapshots of the erosion profiles of the Cu target sputtered at 2.0 Pa. As suggested from the magnetic field configuration given in Fig. 1, the erosion profile of UBMS had a shorter diameter than that of BMS. Thus, in UBMS, the growth of the erosion profile was faster due to the confinement of the applied discharge power over a narrower area. The maximum depth of the profile exceeded 4 mm within 24 h of sputtering in UBMS, while it took 40 h in BMS to reach a similar depth.

From profiles like these, the peak depth, track diameter, (*i.e.*, the separation of erosion peaks in lateral coordinates), and the full-width at half maximum

(FWMH) of the peak were evaluated. On determining the FWHM, we drew a line parallel to the baseline at the half height of the peak depth, and we measured the separation of two intersections between this line and the valley-like profile line. These specific measurements were obtained from the two crossing profiles. Therefore, four data points can be obtained for peak depth and FWHM, while two data points was obtained for track diameter. The typical uncertainties (standard deviation) of the peak depth and FWHM were 0.1 mm. The discrepancy of two track diameters was less than 0.5 mm for the shallower erosion ($<$ 1 mm depth) and was less than 0.3 mm for the deeper erosion ($<$ 3 mm depth).

In addition, the erosion volume was also calculated by assuming axisymmetry of the profile.

[Figure 3 about here.]

Figure 3 displays the sputter time dependence of the peak depth of the erosion profile. The erosion rate was almost linear in all cases and was faster in UBMS than in BMS as shown in Fig. 2. The pressure dependence was relatively subtle, but a slight acceleration of the erosion rate is observed in cases with higher gas pressures.

[Figure 4 about here.]

Figure 4 shows the change in the track diameter as sputtering of the target proceeded. This viewgraph is displayed as a function of the peak depth in order to compare both magnetrons using a similar scale. Note that there is a break in the vertical axis, while the scale is unchanged. The track diameter was confirmed to be shorter in the UBMS case. In addition, the erosion ring in UBMS gradually extended as the sputtering proceeded, while the diameter was unchanged in the BMS cases.

As described earlier, confinement of the plasma by the magnetron is most effective where the magnetic field is parallel to the target surface (*i.e.* $B_z = 0$). In the UBMS magnetron, this position forms a line that gradually shifts from the

symmetric axis as it approach the target surface, which reflects the imbalance in the magnetic flux. Therefore, as the target erosion proceeds, and the target surface decreases, the magnetron plasma shifts outward as a whole. Accordingly, the region of highest ion bombardment also shifts farther from the center of the target. Pressure dependence did not appear at all in the BMS cases. In UBMS, on the other hand, a slightly shorter diameter was obtained at lower gas pressures.

[Figure 5 about here.]

Figure 5 shows the volume of the erosion racetrack as functions of the sputtering time (left) and the peak depth (right). To calculate the volume of the erosion track from its line profile along the target diameter, the profile was approximated as polygonal lines and assumed to be axisymmetric. In some experimental runs, the target mass was also measured when it was removed from the chamber. The discrepancy between the calculated volume and the reduced mass was at most 3%.

From the time dependence (left), we find that the growth rate of the erosion volume was almost the same between UBMS and BMS. In other words, the erosion rate (sputter emission rate) is mostly determined by the target power. Note that the backdeposition of sputtered Cu atoms onto the target surface did not significantly appear in the pressure range used in this study. In conventional sputtering, this backdeposition becomes dominant when the sputtered particles are "thermalized" [35] by the repeated collision and scattering with ambient gas atoms that occurs at higher gas pressures. In the case of Cu, our previous studies [36, 37, 38] suggested that the thermalization of sputtered atoms was not very dominant if the gas pressure was lower than 2 Pa.

From the peak depth dependence (right), we find that the efficiency of the target usage in UBMS is inferior to that in BMS. This is inevitable considering the shorter racetrack diameter of UBMS. Interestingly, the volume versus peak depth relationship exhibited an obvious gas pressure dependence. At higher gas pressures, the growth rate of the volume decelerated as sputtering proceeded,

suggesting that the relative profile of the racetrack changed during the racetrack evolution.

[Figure 6 about here.]

Figure 6 shows the growth of the FWHM of the racetrack as a function of the peak depth. Uncertainties among four measured width values (two profiles were obtained along crossing diameters so four FWMHs could be determined) are shown as error bars in the figure. The FWMH evolution showed a clear dependence on the gas pressure during the sputtering.

The left graph summarizes the UBMS results. The initial width was wider at higher gas pressures. As the erosion proceeded, the width increased slightly at 0.38 Pa, remained mostly constant at 0.50 Pa, and decreased above 1.0 Pa. As a result, the order of the final width was reversed. Namely, higher gas pressure resulted in a narrower track width.

The right graph shows the BMS results. The general trend was similar with UBMS. The initial width was wider at higher gas pressures, but the width decreased faster at higher gas pressures. The final width was reversed from the initial width. However, in comparison with UBMS case, the slopes generally shifted to negative side. In fact, an increase in the width was not observed at the lowest gas pressure condition (0.38 Pa).

[Figure 7 about here.]

To see the evolution of the racetrack shape and to compare its dependency on gas pressure and the magnetron configuration in more detail, the profile snapshots were normalized and plotted. Figure 7 shows the UBMS results. At a gas pressure of 0.38 Pa, the inner side (the side nearer the symmetric axis) of the track was mostly unchanged, while the outer side moved slightly outward. On the other hand, at 2 Pa, both the inner and outer sides shrank, and the profile became significantly narrower. The degree of shrinkage of inner side was greater than that of the outer side.

[Figure 8 about here.]

Figure 8 shows the normalized profile evolution in BMS. At 0.38 Pa, the shape was mostly unchanged, except the outer side moved inward very slightly. This inward movement is the opposite direction of the UBMS case. At 2.0 Pa, both sides of the track shrank evenly, and the track width became narrow.

We can draw the following conclusions about the profile shape evolution: (1) higher gas pressure resulted in a wider initial width; (2) higher gas pressure also resulted in a more rapid decrease in the width shrank as erosion proceeded; and (3) UBMS showed an extending track diameter and (slightly) extending trend of the racetrack width in comparison with BMS. In what follows, we discuss the origins of these behaviors.

For (1), we can consult simulation studies because the target is almost flat at this stage, and the modified target boundary shape is considered to have little effect. Kolev *et al.* applied the PIC-MCC simulation in a cylindrically symmetric system and obtained a monotonic increase of the sputtered flux distribution width with the increase in gas pressure [22] between 0.52–13 Pa. They ascribed this to the increase in the symmetric charge exchange at higher gas pressures.

On the other hand, Buyle *et al.* treated this problem by applying their original model and obtained an opposite trend at a gas pressure ranges lower than 0.5 Pa [17], which was also observed experimentally [39]. Their model categorizes a set of secondary electron orbits as "arches" and depicts electron motion as occasional transports between these arches. This widening of the track at low gas pressures was explained by the relative importance of the secondary electron recapture effect in the inner arches. Though this effect was not confirmed in our measurement at low gas pressures (< 0.5 Pa) within experimental uncertainty, this effect should be considered at lower gas pressure operations.

For (2), the shorter sheath thickness and shorter MFP of secondary electrons can be candidates for the origins of the narrowing trend of the track width at higher gas pressures. If the plasma discharge is generated at a constant power, higher gas pressure usually results in a higher electron density and lower electron temperature. Therefore, the Debye length becomes shorter, and the sheath becomes thinner. As a result, the plasma is more sensitive to the surface groove

generated by the erosion.

[Figure 9 about here.]

Figure 9 shows the dependence of the plasma parameters on gas pressure obtained by the Langmuir probe measurement. The data at each pressure was acquired immediately before the first interval of discharge (2 h). The order of the electron density is comparable with the simulation results by Kolev *et al.* [40] and by Shidoji *et al.* [15] in which the sheath thickness in front of the racetrack was predicted to be on the order of a few millimeters. Okazawa *et al.*used a similar simulation method to Shidoji and obtained a thinner sheath thickness at higher gas pressures [16].

Welzel and Ellmer also suggested that the cathode sheath in a planar magnetron is thinner than the depth of racetrack formed by the magnetron, and follows the shape of erosion profile [41]. They measured the lateral profile of energetic oxygen ions of negative charge in Ar/O_2 reactive sputtering. Their results suggested the ions were emitted at an angle from the target normal, due to the acceleration by the thin cathode sheath covering the slope of the erosion profile. For secondary electrons, thinner sheath thickness also resulted in slanted emission toward the middle of the track from the target surface. This slanted emission should result in "focusing" of the electrons.

In addition, as the erosion proceeded, a stronger magnetic field appears in the discharge space. If the sheath thickness is thin, dense plasma will infiltrate the sheath. This effect was shown by Ido *et al.* [10] in the case of a ferromagnetic target.

The electron MFP is also expected to contribute to the narrowing trend of the erosion profile. According to Sheridan, the total collision MFP at 1 Pa is 1.7 cm and 9.4 cm for 20 eV and 400 eV electrons, respectively [9]. The shorter MFP may result in the occurrence of ionization events nearer the target; hence, the plasma becomes more sensitive to the surface grooves and tends to be confined inside the racetrack.

For (3), the magnetic configuration should explain the gradual widening of the racetrack in the UBMS cases. As shown in Fig. 1, the $B_z = 0$ positions form a curved line in UBMS, which shifts farther from the symmetric axis as it approaches the magnet. Therefore, as the sputter erosion proceeds, the dense plasma, where the majority of ionization occurs, "sweeps" the target surface outward from the center. As a result, the track diameter was extended (Fig. 4), and the track width increased as sputtering proceeds. In contrast, the $B_z = 0$ positions form a straight line that is normal to the target surface in BMS; thus, this effect can be neglected. A similar discussion on the effect of the magnetic configuration on the wider profile width of UBMS was given by Pereira *et al.* [25]. Their discussion can also be applicable in the case of our experiment, in which the hidden part of the $B_z = 0$ line appeared as erosion proceeded.

[Figure 10 about here.]

A comparison of the final profiles with different gas pressures and magnetic configurations is summarized in Fig. 10. For different configurations in UBMS, the inner side of the racetrack apparently differed, while the outer side of the racetrack remained mostly the same. On the other hand, for different configurations in BMS, both sides of the racetrack became narrower as gas pressure increased. These results reflect the summary points (1)–(3) mentioned above.

The experimental observation that the outer side in UBMS was independent on the pressure may be considered from another viewpoint related to the magnetic configuration. Namely, the magnetic field lines emitted from the target surface at $r = 15 \sim 20$ mm, where the outer side of the profile resides in UBMS, does not form a closed loop back to the target surface; the magnetic field lines extended nearly perpendicularly from the target. As a result, the secondary electrons travel along these magnetic field lines and generate ions along this line. Therefore, a similar bombardment flux may be obtained at these radial positions.

In this study, we observed no mounds in the profile. This supports our previous discussion that the backdeposition of the sputtered atoms was not

significant in the parameter range used in this study, and this also means that considerable ion bombardment flux existed in the peripheral of the racetrack which was greater than the backdeposition flux. However, careful observation of the UBMS profiles (left) in Fig. 10 shows that the center part of the profile is found to be slightly shallower at the higher gas pressure cases. This result may be due to the result of increased backdeposition. At higher gas pressures, this effect may become dominant and affect the structure of the erosion profile.

[Figure 11 about here.]

We would like to note a somewhat unusual behavior in the discharge voltage in the course of the sputtering. The dependence of the discharge voltage on the sputtering time is shown in Fig. 11. The discharge voltage had a generally decreasing trend, which can be ascribed to the appearance of a stronger magnetic field in the discharge volume as the target erosion proceeded. The stronger field enhanced the plasma confinement and decreased the discharge impedance.

Interestingly, a voltage maximum also appeared in Fig. 11. The voltage maximum appeared later for higher gas pressures. Comparing the UBMS and BMS cases, the voltage reached its maximum later in the BMS cases. This trend is unchanged even when the voltage was plotted as a function of the erosion depth rather than as a function of the sputter time. The origin of the voltage maximum is not clear at this stage, but it is not specific to the target used in this study. In fact, when we applied the commercially available sputter target in the UBMS case at 2.0 Pa, a similar maximum also appeared (shown as a dotted line in Fig. 11). Because the erosion depth at the voltage maximum reached as much as 1 mm in several cases, it may not be related to the removal of the affected layer introduced by the machining. We suspect the possible origins of the voltage maximum are roughening of the target surface by sputtering or some local condition of plasma generation, but further study will be necessary.

Finally, we would like to note that the discharge power of 100 W used in this study was very low. This discharge power corresponded to the discharge power density of 2.3W/cm^2 by dividing the power by the area of the 75-mm-

diameter target. The erosion profile is considered to be dependent on the target power. For example, Clarke *et al.*reported that the broader profile was obtained in the case of High power Impulse Magnetron Sputtering (HiPIMS) compared to conventional DC sputtering [42]. The difference in target power should result in a different plasma structure, and should lead to a different erosion profile.

4. Summary

We measured the evolution of the target erosion profile for both unbalanced and balanced magnetron sputtering at different gas pressures with a constant discharge power of 100 W. The racetrack was formed under positions where the magnetic field is parallel to the target surface and reflected the magnetic configuration. When the backdeposition of sputtered atoms did not play an important role, growth of the erosion volume was found to be nearly almost identical regardless of the magnetic field configuration and gas pressures. Hence, smaller track diameters lead to the faster growth of the erosion peaks and inferior target usage efficiency.

The track width changed as sputtering erosion proceeded: (1) higher gas pressure resulted in a wider initial width; (2) higher gas pressure resulted in a more rapid decrease in the width as erosion proceeded; and (3) UBMS showed the extending track diameter and extending trend of the racetrack width in comparison with BMS. These results occur because the plasma behavior reflected the gas pressure and magnetic configuration. Finally, the magnetron plasma for sputtering is affected by the target erosion, which should be treated as a change in the boundary conditions.

Acknowledgment

We gratefully acknowledge PEGASUS Software Inc. for financial support. We also wish to thank Yuuki Kadoi and Ryuhei Kamata for their assistance with the experiments. Furthermore, we acknowledge the helpful comments and suggestions of unknown reviewers.

References

[1] J. S. Chapin, The planar magnetron, Research/Development, Vacuum Technology 25 (1974) 37–40.

[2] J. S. Chapin, Sputtering process and apparatus, U.S. Patent No. 4,166,018, 1979. URL: `http://www.google.co.jp/patents/US4166018`.

[3] J. Musil, Recent advances in magnetron sputtering technology, Surf. Coat. Technol. 100-101 (1998) 280–286.

[4] P. J. Kelly, R. D. Arnell, Magnetron sputtering: a review of recent developments and applications, Vacuum 56 (2000) 159–172.

[5] J. G. Han, Recent progress in thin film processing by magnetron sputtering with plasma diagnostics, J. Phys. D: Appl. Phys. 42 (2009) 043001.

[6] G. Bräuer, B. Szyszka, M. Vergöhl, R. Bandorf, Magnetron sputtering Milestones of 30 years, Vacuum 84 (2010) 1354–1359.

[7] W. D. Westwood, Sputter Deposition, AVS, New York, New York, 2003.

[8] K. Wasa, S. Hayakawa, Handbook of sputter deposition technology, Noyes Publications, New Jersey, 1992.

[9] T. E. Sheridan, M. J. Goeckner, J. Goree, Model of energetic electron transport in magnetron discharges, J. Vac. Sci. Technol. A 8 (1990) 30–37.

[10] S. Ido, T. Suzuki, M. Kashiwagi, Computational studies on the erosion process in a magnetron spu ttering system with a ferromagnetic target, Jpn. J. Appl. Phys. 37 (1998) 965–969.

[11] S. Ido, M. Kashiwagi, M. Takahashi, Computational Studies of Plasma Generation and Control in a Magnetron Sputtering System, Jpn. J. Appl. Phys. 38 (1999) 4450–4454.

[12] E. Shidoji, M. Nemoto, T. Nomura, Y. Yoshikawa, Three-dimentional simulation of target erosion in DC magnetron sputtering, Jpn. J. Appl. Phys. 33 (1994) 4281–4284.

[13] Q. H. Fan, D. Galipeau, L. Q. Zhou, J. J. Gracio, Computer-aided development of a magnetron source with high target utilization, Vacuum 85 (2011) 833–838.

[14] E. Shidoji, H. Ohtake, N. Nakano, T. Makabe, Two-dimensional self-consistent simulation of a DC magnetron discharge, Jpn. J. Appl. Phys. 38 (1999) 2131–2136.

[15] E. Shidoji, N. Nakano, T. Makabe, Numerical simulation of the discharge in d.c. magnetron sputtering, Thin Solid Films 351 (1999) 37–41.

[16] K. Okazawa, E. Shidoji, T. Makabe, Prediction of the evolution of the erosion profile in direct current magnetron discharge, J. Appl. Phys. 86 (1999) 2984–2989.

[17] G. Buyle, D. Depla, K. Eufinger, J. Haemers, R. De Gryse, W. De Bosscher, Simplified model for calculating the pressure dependence of a direct current planar magnetron discharge, J. Vac. Sci. Technol. A 21 (2003) 1218–1224.

[18] T. M. Minea, J. Bretagne, G. Gousset, L. Magne, D. Pagnon, M. Touzeau, PIC-MCC simulation of a r.f. planar magnetron discharge and comparison with experiment, Surf. Coat. Technol. 116-119 (1999) 558–563.

[19] C. Shon, J. Lee, Modeling of magnetron sputtering plasmas, Appl. Surf. Sci. 192 (2002) 258–269.

[20] I. Kolev, A. Bogaerts, R. Gijbels, Influence of electron recapture by the cathode upon the discharge characteristics in dc planar magnetorons, Phys. Rev. E 72 (2005) 056402.

[21] E. Bultinck, A. Bogaerts, The effect of the magnetic field strength on the sheath region of a dc magnetron discharge, J. Phys. D: Appl. Phys. 41 (2008) 202007.

[22] I. Kolev, A. Bogaerts, Numerical study of the sputtering in a dc magnetron, J. Vac. Sci. Technol. A 27 (2009) 20–28.

[23] S. Kadlec, Computer simulation of magnetron sputtering – Experience from the industry, Surf. Coat. Technol. 202 (2007) 895–903.

[24] A. Bogaerts, E. Bultinck, I. Kolev, L. Schwaederlé, K. Van Aeken, G. Buyle, D. Depla, Computer modelling of magnetron discharges, J. Phys. D: Appl. Phys. 42 (2009) 194018.

[25] P. J. S. Pereira, M. L. Escrivão, M. R. Teixeira, M. J. P. Maneira, Y. Nunes, Analytical model and measurements of the target erosion depth profile of balanced and unbalanced planar magnetron cathodes, Plasma Sources Sci. Technol. 23 (2014) 065031.

[26] T. Fukami, T. Sakuma, Target Erosion Pattern in Planar Magnetron Sputtering, Jpn. J. Appl. Phys. 21 (1982) 1680–1683.

[27] T. Fukami, F. Shintani, M. Naoe, Observations on the operation of a planar magnetron sputtering system by target erosion patterns, Thin Solid Films 151 (1987) 373–381.

[28] J. Musil, K. Rusák, V. Ježek, J. Vlček, Planar magnetron with additional plasma confinement, Vacuum 46 (1995) 341–347.

[29] J. Musil, Rectangular magnetron with full target erosion, J. Vac. Sci. Technol. A 17 (1999) 555 – 563.

[30] W. De Bosscher, H. Lievens, Advances in magnetron sputter sources, Thin Solid Films 351 (1999) 15–20.

[31] T. Iseki, Target utilization of planar magnetron sputtering using a rotating tilted unbalanced yoke magnet, Vacuum 84 (2009) 339–347.

[32] T. Iseki, Completely flat erosion magnetron sputtering using a rotating asymmetrical yoke magnet, Vacuum 84 (2010) 1372–1376.

[33] T. Nakano, Y. Saitou, M. Ueda, N. Itamura, S. Baba, Growth of Target Race Track Profile during Magnetron Sputtering, J. Vac. Soc. Jpn. 58 (2015) 261–264.

[34] H. H. Andersen, H. L. Bay, Sputtering Yield Measurements, in: R. Behrisch (Ed.), Sputtering by Particle Bombardment I, Springer-Verlag, Berlin, 1981, pp. 145–218.

[35] G. M. Turner, I. S. Falconer, B. W. James, D. R. McKenzie, Monte Carlo calculation of the thermalization of atoms sputtered from the cathode of a sputtering discharge, J. Appl. Phys. 65 (1989) 3671–3679.

[36] T. Nakano, S. Baba, Gas pressure effects on thickness uniformity and circumvented deposition during sputter deposition process, Vacuum 80 (2006) 647–649.

[37] T. Nakano, R. Yamazaki, S. Baba, Effects of Atomic Weight, Gas Pressure, and Target-to-substrate Distance on Deposition Rates in the Sputter Deposition Process, J. Vac. Soc. Jpn. 57 (2014) 152–154.

[38] T. Nakano, S. Baba, Estimation of the pressuredistance product for thermalization in sputtering for some selected metal atoms by Monte Carlo simulation, Jpn. J. Appl. Phys. 53 (2014) 038002.

[39] G. Buyle, D. Depla, K. Eufinger, J. Haemers, R. D. Gryse, W. D. Bosscher, B. Advanced, C. Bekaert, Influence of Recapture of Secondary Electrons on the Magnetron Sputtering Deposition Process, in: Proc. 45th SVC Annu. Tech. Conf., 2002, pp. 348–353.

[40] I. Kolev, A. Bogaerts, PIC MCC Numerical Simulation of a DC Planar Magnetron, Plasma Process. Polym. 3 (2006) 127–134.

[41] T. Welzel, K. Ellmer, The influence of the target age on laterally resolved ion distributions in reactive planar magnetron sputtering, Surf. Coat. Technol. 205 (2011) S294–S298.

[42] G. Clarke, A. Mishra, P. J. Kelly, J. W. Bradley, Cathode Current Density Distributions in High Power Impulse and Direct Current Magnetron Sputtering Modes, Plasma Process. Polym. 6 (2009) S548–S553.

List of Figures

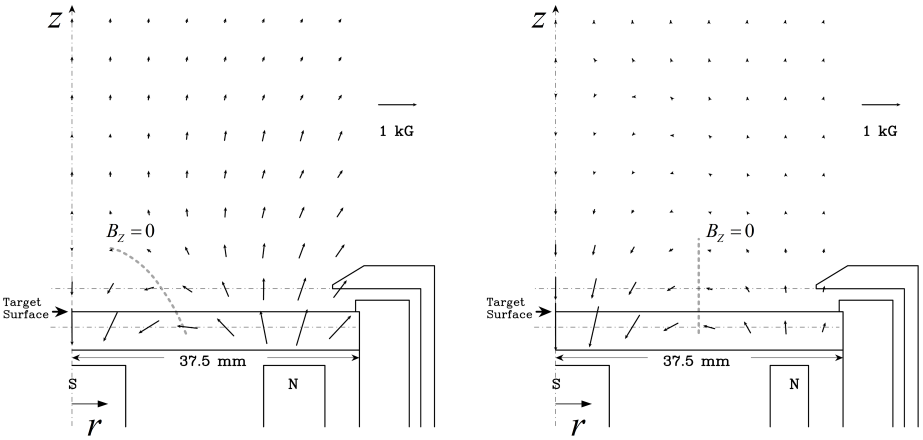

Figure 1: Vector maps of the magnetic flux around the magnetron target. Left: unbalanced magnetron sputtering (UBMS) system, Right: balanced magnetron sputtering (BMS) system. Each arrow denotes the magnetic flux vector at the center of the arrow. Arrows are arranged in 5-mm steps in both the vertical and radial directions. Dotted lines denote the locations where the magnetic field is parallel to the target surface ($B_z = 0$).

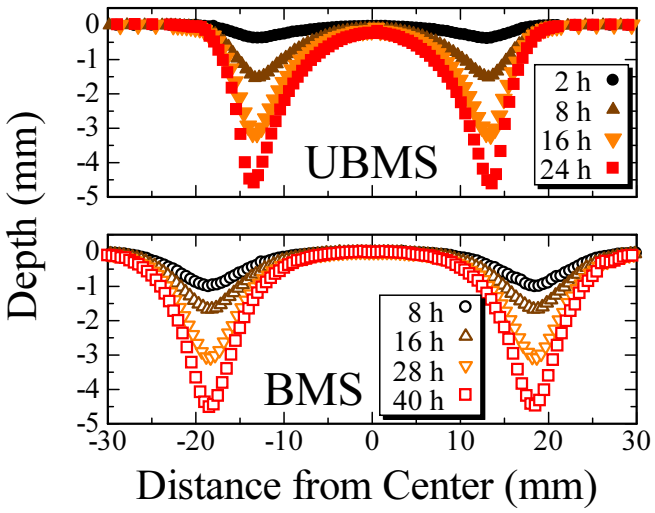

Figure 2: Examples of the erosion profile evolution: Cu target sputtered at 2.0 Pa and DC power of 100 W. Upper: unbalanced magnetron sputtering (UBMS) configuration, Lower: balanced magnetron sputtering (BMS) configuration.

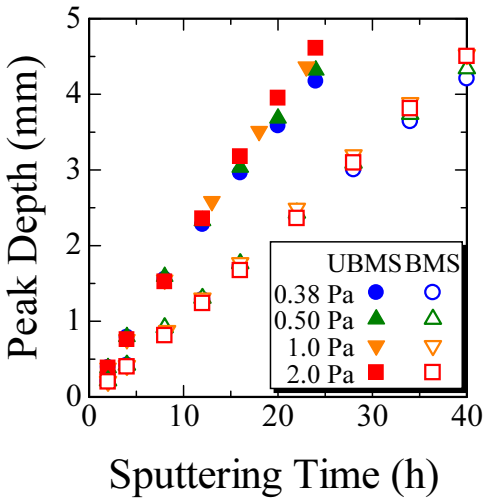

Figure 3: Sputtering time dependence of the peak depth of the erosion profiles of Cu targets

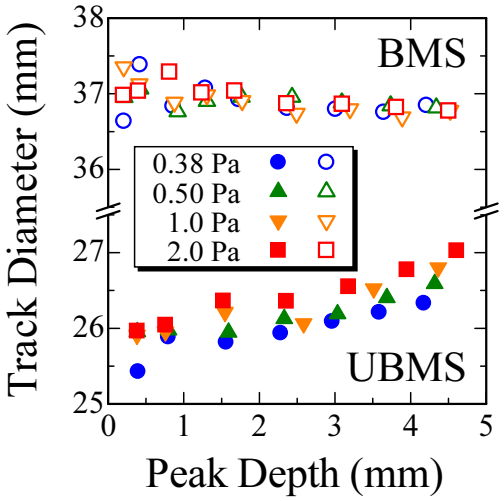

Figure 4: Dependence of the track diameter (the distance between the peaks of the profile) on the peak depth. Note the break in the vertical axis. The scale is unchanged.

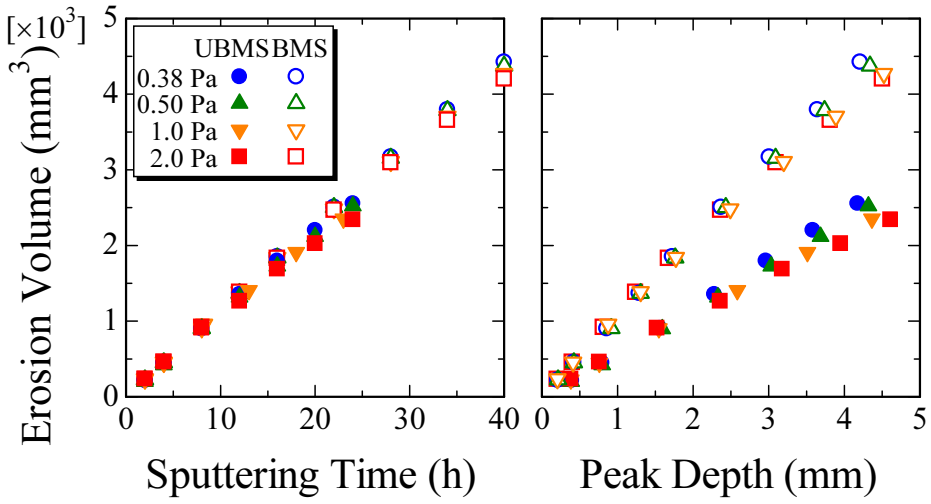

Figure 5: Dependence of the erosion volume on the sputtering time (left) and peak depth (right).

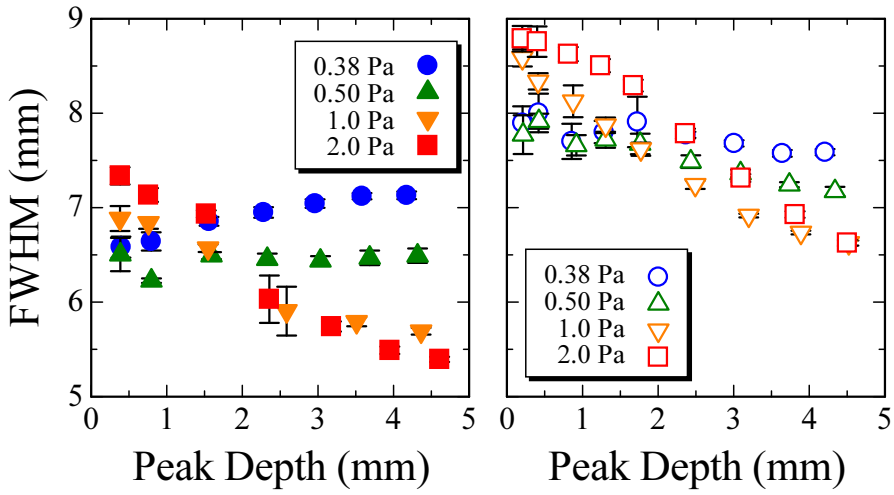

Figure 6: FWHM of the racetrack as a function of the peak depth. Data plots are accompanied by error bars denoting the standard deviation of the four values obtained at each snapshot; however, most of the error bars are hidden behind the plot.

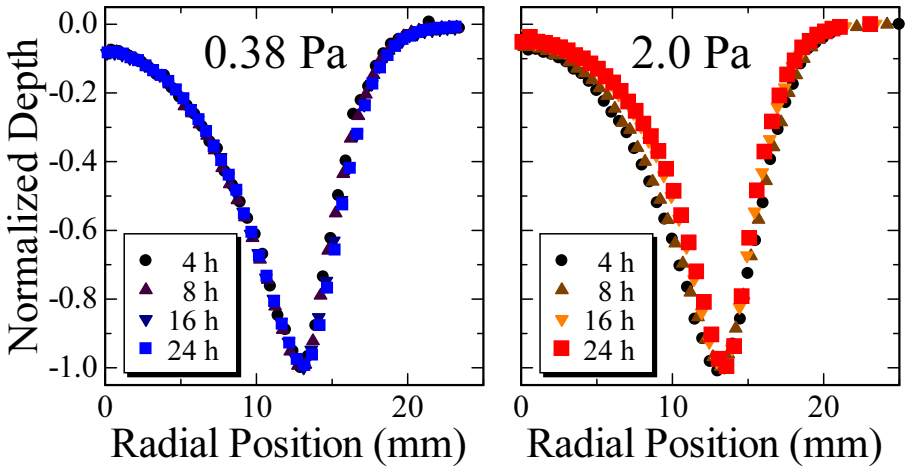

Figure 7: Transient evolution of the erosion profile for the UBMS target at 0.38 Pa (left) and at 2.0 Pa (right).

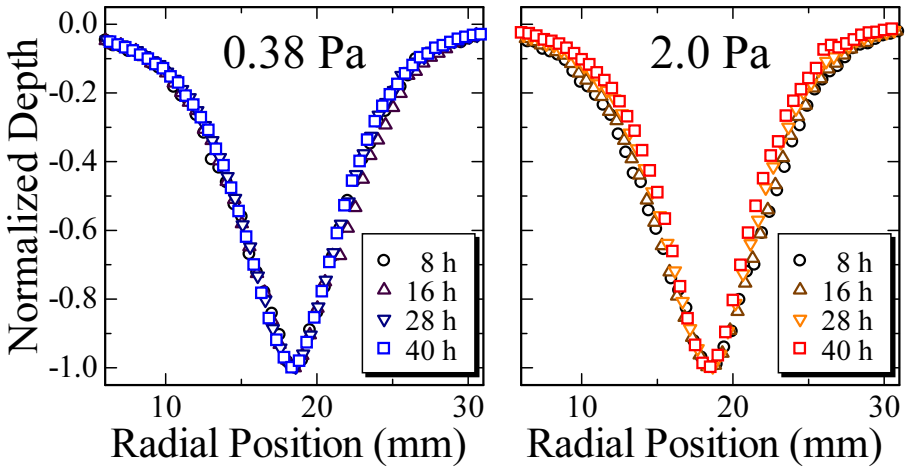

Figure 8: Transient evolution of the erosion profile for the BMS target at 0.38 Pa (left) and at 2.0 Pa (right).

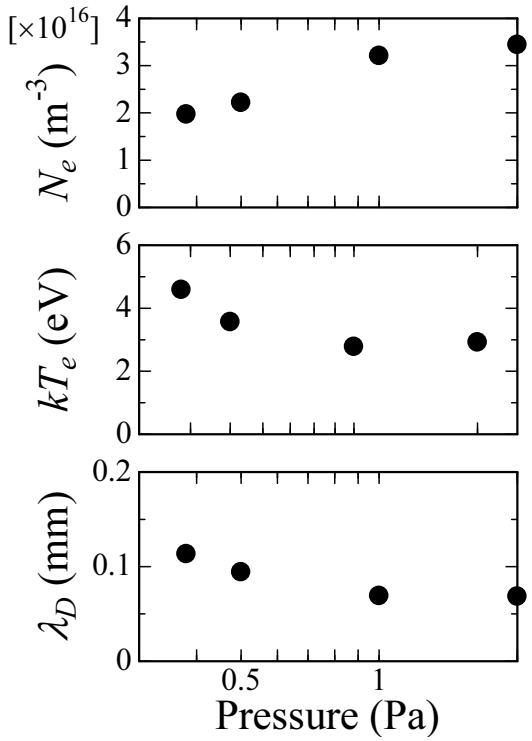

Figure 9: Pressure dependence of the plasma parameters (from top: electron density, electron temperature, and the Debye length) measured by the Langmuir probe whose apex was located 10 mm from the target surface.

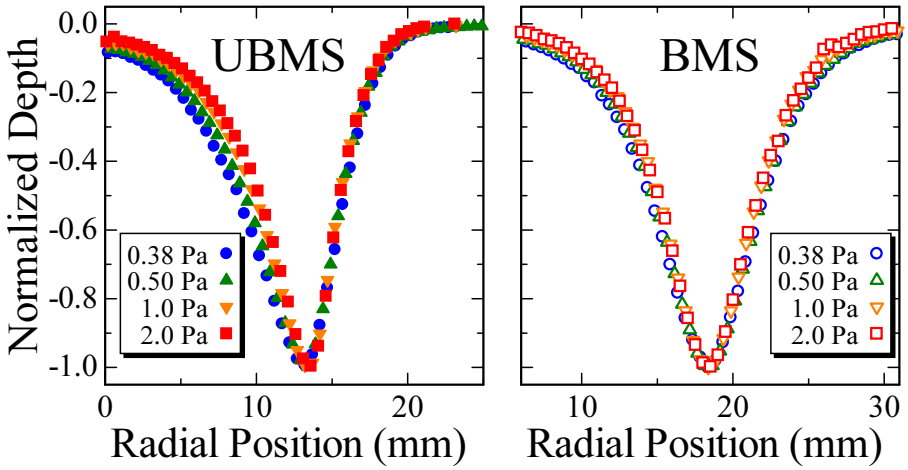

Figure 10: Final profiles of the erosion track for UBMS (left) and BMS (right).

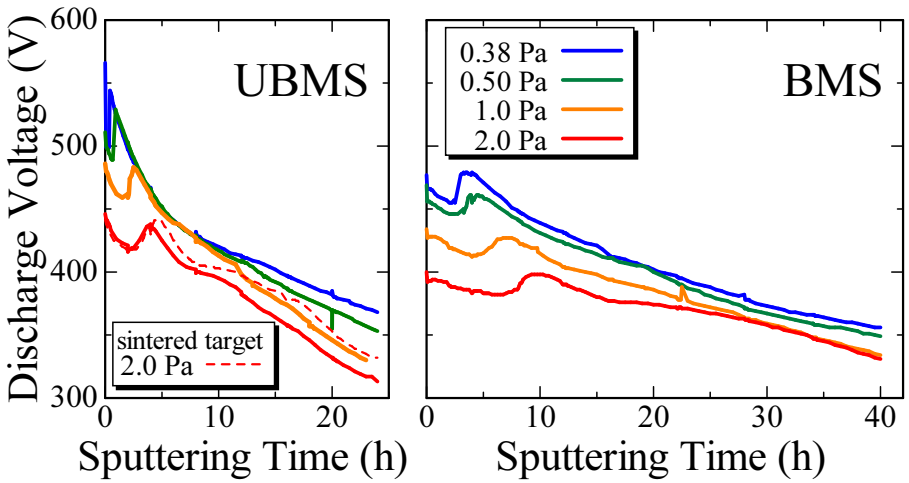

Figure 11: Discharge voltage during sputtering. The dashed line denotes the result of the commercially available (sintered) sputtering target. The other lines show the results of the target sliced from a Cu rod and polished.